NEOPLASIA
www.neoplasia.com

Volume 14 Number 4 April 2012 pp. 259–270 259

Differential Roles of uPAR in Peritoneal Ovarian Carcinomatosis[1,2]

Nada N. Al-Hassan*, Ali Behzadian†, Ruth Caldwell†, Vessela S. Ivanova‡, Viqar Syed‡, Kouros Motamed§ and Neveen A. Said*

*Department of Urology, University of Virginia School of Medicine, Charlottesville, VA, USA; †Vascular Biology Center, Georgia Health Science University, Augusta, GA, USA; ‡Department of Obstetrics and Gynecology, Uniformed Services University of the Health Sciences, Bethesda, MD, USA; §Biomiga Diagnostics, Fountain Valley, CA, USA

Abstract

Epithelial ovarian cancer is the fourth leading cause of death from gynecologic malignancies in the United States. Most cases are diagnosed at late stages, with the solid tumor masses growing as peritoneal implants, or floating within the ascitic fluid (peritoneal ovarian carcinomatosis). Despite aggressive surgical "debulking," recurrence of recalcitrant disease is frequent with poor patient survival. Efforts to improve survival rates are hindered by lack of biomarkers that can detect and effectively treat ovarian cancer in its early stages. Urokinase plasminogen activator receptor (uPAR) is a multifunctional receptor involved in a myriad of tumor cell processes. However, the role of host uPAR in ovarian cancer is still elusive. To define the potential proinflammatory role of uPAR in ovarian cancer, first, using a syngeneic murine model in *uPAR*$^{-/-}$ mice, we found that ablation of uPAR restrained tumor take and peritoneal implants and prolonged the survival of *uPAR*$^{-/-}$ mice compared with their *uPAR*$^{+/+}$ counterparts. Ascitic fluid accumulation was significantly decreased in *uPAR*$^{-/-}$ mice with decreased macrophage infiltration. Second, *in vitro* mechanistic studies revealed that host uPAR is involved in the multiple steps of peritoneal metastatic cascade. Third, we evaluated the prognostic utility of tumor and stromal uPAR in human ovarian cancer tissue microarray. In summary, our studies indicated that uPAR plays a significant role in ovarian cancer cell-stromal crosstalk and contributes to increased vascular permeability and inflammatory ovarian cancer microenvironment. This provides a rationale for targeting the uPAR with either specific neutralizing antibodies or targeting its downstream inflammatory effectors in patients with ovarian cancer.

Neoplasia (2012) 14, 259–270

Introduction

Ovarian cancer is the fourth leading cause of cancer death among US women [1]. It has the highest mortality rate of all gynecologic tumors because most patients will experience recurrences and develop chemoresistant disease [1]. Unlike other invasive metastasizing tumors, disseminated ovarian cancer cells have predilection to peritoneal cavity where they survive as floating spheroids or implants onto peritoneal surfaces [2]. The first step of peritoneal metastasis involves a tightly regulated multistep process of detachment, migration, invasion of, and, proliferation on, mesothelium-covered surfaces [2,3]. A number of factors have been implicated as mediators of ovarian cancer metastasis, including proteases [4].

Address all correspondence to: Neveen A. Said, MD, PhD, Department of Urology, University of Virginia School of Medicine, 1300 Jefferson Park Ave, Jordan Hall #2-11B, Charlottesville, VA 22908. E-mail: ns8v@virginia.edu

[1]This study was supported in part by Paul Mellon Foundation startup fund from the University of Virginia School of Medicine to N.A.S., the Georgia Cancer Coalition (grant GCC0023) to K.M., and National Institutes of Health grant CA123558 to V.S.
[2]This article refers to supplementary materials, which are designated by Figures W1 and W2 and are available online at www.neoplasia.com.
Received 26 February 2012; Revised 19 March 2012; Accepted 29 March 2012

DOI 10.1593/neo.12442

The urokinase plasminogen activator receptor (uPAR) was originally identified on the monocyte/macrophage–like human cell line U937 as the membrane receptor for the serine protease urokinase-type plasminogen activator (uPA) and has since been implicated in a large number of physiological and pathologic conditions, including cancer invasion and metastasis [5]. In addition to mediating directed extracellular proteolysis on the surface of migrating or invading cells, uPAR also mediates cell signaling, proliferation, and survival [6–8]. Highly endogenous intratumoral levels of both uPAR and its ligand uPA are often present in advanced metastatic cancers (summarized in Mazar [7]). uPAR is expressed in tumors by multiple tumor-associated cell types including the tumor cells themselves, endothelial cells, stromal cells and tumor-associated macrophages (TAMs) [7,9,10]. In patients with ovarian cancer, high levels of uPA, soluble uPAR, and/or uPAR have been detected in serum, ascites, and ovarian cancer tumors (primary and metastatic; summarized in Kenny et al. [6]), whereas the prognostic utility of uPAR expression in ovarian cancer tumor tissues was not established [6]. However, mechanistic studies revealed that targeting uPAR by a neutralizing antibody inhibited ovarian cancer cell adhesion, invasion, and migration *in vitro* and reduced tumor burden in *in vivo* xenografts [6].

The uPA/uPAR axis also plays a critical role in monocyte and macrophage chemotaxis [8,11]. In the peritoneal microenvironment, inflammatory and proteolytic factors present as a major component and are contributed not only by invasive tumor cells but also by a large number of infiltrating macrophages (TAMs), activated mesothelial cells, and endothelial cells [12–14].

uPAR, through binding to its agonist uPA, initiates plasmin-mediated extracellular cell matrix (ECM) proteolysis, which is involved in many processes in which cell migration occurs, including tumor cell invasion [15] and monocyte infiltration [16]. uPA/uPAR axis has been shown to stimulate adhesion and chemotactic movement of myeloid cells [17] and to induce cell migration in human endothelial cells [18].

Independently of its proteolytic activity, uPAR has been shown to interact with integrins, ECM molecules vitronectin, laminin, and fibronectin with activation of growth factor receptors, and integrin signaling cascades that converge in cell survival, adhesion, migration, invasion, and angiogenesis [6,11,19–21].

The involvement of uPAR in vascular endothelial growth factor (VEGF)–induced angiogenesis and tumor cell invasiveness has been earlier reported in meningiomas, gliomas, and glioblastomas and was contributed by endothelial cells as well as tumor cells [19,20,22]. In addition, uPAR has been identified as a downstream effector of VEGF-induced microvascular permeability, a process that involved VEGF receptor 2 (VEGFR2) tyrosine phosphorylation, disruption of endothelial tight junction proteins, and β-catenin nuclear translocation [23,24].

To gain insight on the multifunctional properties of the uPAR in ovarian cancer, and given that antibody-based therapies have been established as clinically feasible and efficacious [6], we decided to investigate the differential effects of host uPAR in the peritoneal microenvironment. We first used a syngeneic murine model of ovarian cancer injecting ID8 cells [25–27] in $uPAR^{-/-}$ and $uPAR^{+/+}$ mice [8]. We dissected the contribution of uPAR from each cell type *in vitro* in primary and established human cells first to identify the roles of host uPAR and to verify that the observed biologic functions are specific to the molecule independent of the host background or the long-term knockdown of the uPAR. To our knowledge, this is the first report that demonstrates a direct link between activation of host uPAR, TAM, and vascular permeability in ovarian cancer.

Materials and Methods

Mice

Homozygous $uPAR^{-/-}$ and $uPAR^{+/+}$ (C57B6 background) were from Jackson Laboratories (Bar Harbor, ME). Mice were backcrossed on C57B6 background. uPAR deficiency does not compromise fertility or development [28]. All experimental procedures were performed according to the approved Institutional Animal Care and Use Committee protocols of Medical College of Georgia.

In Vivo *Tumor Generation and Fluorescent Stereomicroscopy*

For intraperitoneal (IP) tumor generation, ID8 cells stably expressing GFP and GFP-VEGF [14,26] were injected in $uPAR^{+/+}$ and $uPAR^{-/-}$ mice (n = 15 per group). Animals were monitored twice weekly for tumor development and survival (up to 15 weeks). Tumor growth was determined by weekly measurements of animal girth [14,26]. At the end of the experimental period (8 weeks), animals were sacrificed, and organs were examined for tumor development and spread. The gross morphology of tumor growth and the extent of dissemination in the peritoneal cavity were observed and documented using a fluorescent stereomicroscope equipped with Q-Imaging digital camera (Leica Microsystems, Wetzlar, Germany) [26]. Tumor dissemination in the peritoneal cavity was scored on two arbitrary scales based on the number and size of tumor nodules as earlier described [26]. On the basis of tumor nodule size, each animal was given an arbitrary score from 0 to +4 (0, for tumor-free animals with undetectable nodular growths; +1, for nodules <1 mm in diameter or those only visualized by fluorescent stereomicroscopy; +2, for nodules 1-5 mm in diameter, +3, for nodules 5-10 mm; and +4, for nodules >10 mm). On the basis of the number of nodules in the peritoneal surface and abdominal structures, another scale from 0 to +4 was set (0, for tumor free; +1, for 0-5 nodules/examined organ, including nodules that were only detected by fluorescent stereomicroscope; +2, for 5-10 nodules/organ; +3, for 10-15 nodules; +4, for >20 nodules including nodular plaques and omental caking). Results were expressed as the mean score ± SEM for each animal. Tissues and ascitic fluid were collected and processed as earlier described [14,26].

Cell Lines and Reagents

Human ovarian carcinoma cell lines (SKOV3, OVCAR3, and CAOV3), human peritoneal mesothelial cell line (Meso301), murine ovarian carcinoma cell line (ID8), and human monocytoid cell line (U937) were obtained from ATCC (Manassas, VA) and maintained as described previously [14,26,29,30]. Human umbilical vein endothelial cells (HUVECs) were purchased from Lonza (Walkersville, MD) and were maintained in endothelial cell growth media as per supplier instructions. Reduced growth factor Matrigel was from BD Biosciences (Bedford, MA). Recombinant human VEGF was from Peprotech (Rocky Hill, NJ). Human uPAR MAb (clone 62022) was from R&D Systems (Minneapolis, MN). Unless otherwise stated, all other chemicals and culture media were purchased from Sigma (St. Louis, MO) and Thermo Fisher Scientific (Fairlawn, NJ).

Transfections, Western Blot Analysis, and Gelatin Zymography

Knockdown of uPAR in mesothelial cells, HUVECs, and U937 macrophages was carried out using ON-TARGETplus SMARTpool Human PLAUR small interfering (siRNA) oligonucleotides (Dharmacon, Millipore, Billerica, MA) and FuGENE 6 transfection reagent (Roche, Branchburg, NJ). The efficiency of transfection was determined

48 hours later by harvesting cells in RIPA buffer as earlier described [27,31,32]. Protein concentrations were determined by bicinchoninic acid (BCA) assay (Pierce, Thermo Fisher). Cell lysates (25 μg) were resolved by 4% to 20% SDS-PAGE, and transferred onto polyvinylidene fluoride (PVDF) membranes (BioRad, Hercules, CA) and probed with the indicated antibodies. Protein detection was carried out using HRP-conjugated secondary antibodies and SuperSignal Femto Maximum Sensitivity Substrate (Pierce). For zymography, ascitic fluid was cleared by centrifugation at 12,000*g* for 20 minutes at 4°C, 10 μg was resolved in 10% SDS-PAGE gels containing 1 mg/ml gelatin under nonreducing conditions, and gelatinolytic activity was detected in Coomassie blue–stained gels [26].

Luciferase Activity Assays

Mesothelial cells, HUVECs, and U937 cells (5×10^4/well of a 24-well plate) were transfected with 0.5 μg of pNFκB-Luc (Stratagene, La Jolla, CA) using FuGENE 6, 24 hours after transfection with si uPAR or scrambled (scr) control oligonucleotides, as per manufacturer's instructions, serum starved for an additional 24 hours, and were cocultured with the ovarian cancer cells for further 24 hours before lysis (Glo Lysis Buffer; Promega, Madison, WI). Luciferase activity was measured (Luciferase Assay Solution, Bright Glo; Promega) and were normalized by measuring DNA content of cells using CyQuant cell proliferation assay (Molecular Probes, Eugene, OR), according to the manufacturer's protocol.

Preparation of Conditioned Medium

Subconfluent monolayers of human ovarian cancer cells and U937 macrophages (2×10^6 cells/well), were grown in six-well plates, serum starved in serum-free medium overnight, and were allowed to condition for 72 hours. Conditioned media (CM) were collected and cleared by centrifugation, filter sterilized, and added to the bottom chambers for chemoinvasion assays.

Cytokines, Prostaglandin E_2, and 8-Isoprostane ELISA and uPA Activity

The levels of VEGF, IL-6, CCL2, and 8-isoprostane and prostaglandin E_2 (PGE_2) were determined in the ascitic fluid and CM of different experimental conditions using appropriate species-specific commercial kits from R&D Systems, Cayman Chemical, Inc (Ann Arbor, MI), and RayBiotech, Inc (Norcross, GA), as per the manufacturer's recommendations. uPA activity was measured by a colorimetric assay kit (Chemicon, Millipore), according to the supplier's guidelines. The assay is sensitive over a range of 0.05 to 50 U of uPA activity, which cleaves a chromogenic substrate, a tripeptide with pNA group, forming a colored product with detectable absorbance at A_{405}.

Adhesion and Invasion Assays

Ovarian cancer cell lines were labeled with CellTracker Green CMFDA (5-chloromethylfluorescein diacetate; Molecular Probes, Invitrogen) as per manufacturer's instructions and were allowed to adhere to confluent monolayers of Meso301 cell lines as earlier described [14,30]. Chemoinvasion assays were carried out with 24-well 3- and 8-μm-pore-size polycarbonate filters (Costar, Corning, NY) coated with Matrigel. Briefly, 1×10^5 cells were added to the upper chambers of Matrigel-coated filters, and the bottom chambers were filled with 600 μl of 72-hour CM of cancer cells or macrophages. Chemoinvasion assays were carried out for 5 hours, at the end of which cells that migrated to the undersurface of the filters were stained with Diff-Quick (Fisher Scientific), and cells were counted in six high-power fields as described earlier [14,26,27,29–32].

Immunohistochemistry of Murine Tissues and Human Tissue Microarrays

Ki67 and F4/80 antibodies were purchased from BD Biosciences and AbD Serotec Protein (Raleigh, NC). F4/80 and proliferation indices were determined [26,32]. Human ovarian cancer tissue microarrays (TMAs) were purchased from US Biomax (Bethesda, MD). uPAR protein intensity and frequency were detected in human TMAs and were blindly scored by two independent investigators. The intensity of the staining was categorized from negative (–) to low (+), intermediate (++), and high (+++). The frequency of staining was determined by counting the number of positive cells divided by 100 cells. The cutoffs of expression for prognostic evaluation were selected based on the median values of expression among the groups under analysis [32]. The two scoring systems were adopted because of tumor heterogeneity and based on the assumption that increase in intensity of uPAR protein expression likely precedes increases in its frequency and therefore should have a higher weight. For each core, data were transformed into composite expression score CES the intensity + frequency. The range of CES was from 0 to 12 for tumor uPAR and from 0 to 4 for stromal uPAR.

RNA Isolation and Quantitative Reverse Transcription–Polymerase Chain Reaction

Total RNA was extracted from cultured cells RNeasy kits (Qiagen, Valencia, CA) and quantitative reverse transcription–polymerase chain reaction was carried out using iScript cDNA Synthesis Kit and iQ SYBR Green SuperMix and BioRad iCycler. The primer sequences for human VEGF were F, 5′-ctacctccaccatgccaagt-3′, and R, 5′-gcagtagctgcgctgataga-3′; those for human CCL2 were F, 5′-cagccagatgcaatcaatgc-3′, and R, 5′-gcactgagatcttcctattggtgaa-3′; and those for human IL-6 were F, 5′-ggtacatcctcgacggcatct-3′, and R, 5′-gtccctctttgctgcttcac-3′. The primer sequences for GAPDH were F, 5′-agggctgctttaactctggt-3′, and R, 5′-ccccacttgattttggaggga-3′. Each analysis was performed in triplicate.

Measurement of Paracellular Flux

HUVECs (2×10^5 cells/well) were seeded on 24-well filters (0.4 μm, 6.5-mm transparent polycarbonate filters) and allowed to attach and form tight junctions for 48 hours in complete growth medium. HUVECs were then shifted to serum-free medium for 24 hours then were treated with VEGF (40 ng/ml) or for 72 hours with CM of ovarian cancer cells. The paracellular flux is measured by adding 0.5 mg/ml fluorescein isothiocyanate–conjugated dextran (FITC-dextran; M_r = 5000; Sigma) in the apical chamber before and after apical treatment of cells with, as well as CM of ovarian cancer cell lines. Measurements were made before treatment and at 1, 2, 4, and 6 hours after treatment. Transmembrane flux of dextran 5K from apical to basal was determined by measuring the fluorescence in the 10-μl aliquots taken from both apical and basal compartments at 496 nm. The rate of permeation was determined by the ratio of apical/basal fluorescence [33,34]. To determine whether blocking uPAR will abrogate the permeability-inducing effect of VEGF and CM, HUVECs were preincubated with 10 μm/ml anti-uPAR Ab for 1 hour before adding VEGF or CM to the upper chambers.

Immunofluorescence Staining of the Tight Junction Protein Zona Occludens 1

At the beginning and at the indicated time points of the endothelial permeability experiments described, HUVECs on filters were washed three times with PBS and fixed in absolute methanol at −20°C for 15 minutes, permeabilized with 0.02% Tween 20 in PBS for 10 minutes, and blocked with 20% AquaBlock (East Coast Biologics, Inc, North Berwick, MA) in PBS for 3 hours. Filters are then incubated with FITC–zona occludens 1 (ZO-1) antibody (Chemicon, Millipore) diluted in blocking buffer for 1 hour at room temperature. After further washing, the filters are mounted with Vectashield Mounting Medium (Vector Lab, Burlingame, CA) and examined under a fluorescent microscope.

Statistical Analysis

Kaplan-Meier curves, 2 × 2 Fisher exact test, and χ^2 test and nonparametric Wilcoxon-Mann-Whitney analysis of IP tumors and the association of the expression of uPAR with histopathologic tumor grade were evaluated using the nonparametric Wilcoxon-Mann-Whitney and Kruskal-Wallis tests, performed using GraphPad Prism 5.0 (San Diego, CA). Differences were considered significant at $P < .05$. All other data were analyzed by two-tailed Student's t test and one-way analysis of variance (ANOVA).

Results

Suppression of Peritoneal Ovarian Carcinomatosis in uPAR$^{-/-}$ *Mice*

Using a syngeneic mouse model of peritoneal ovarian carcinomatosis (POC) injecting ID8-GFP murine ovarian cancer cell line [26] in *uPAR*$^{-/-}$ mice and their wild-type (*uPAR*$^{+/+}$) littermates, we found prolonged survival (Figure 1*A*) and restrained tumor growth in *uPAR*$^{-/-}$ mice compared with their wild-type counterparts. Disease progression

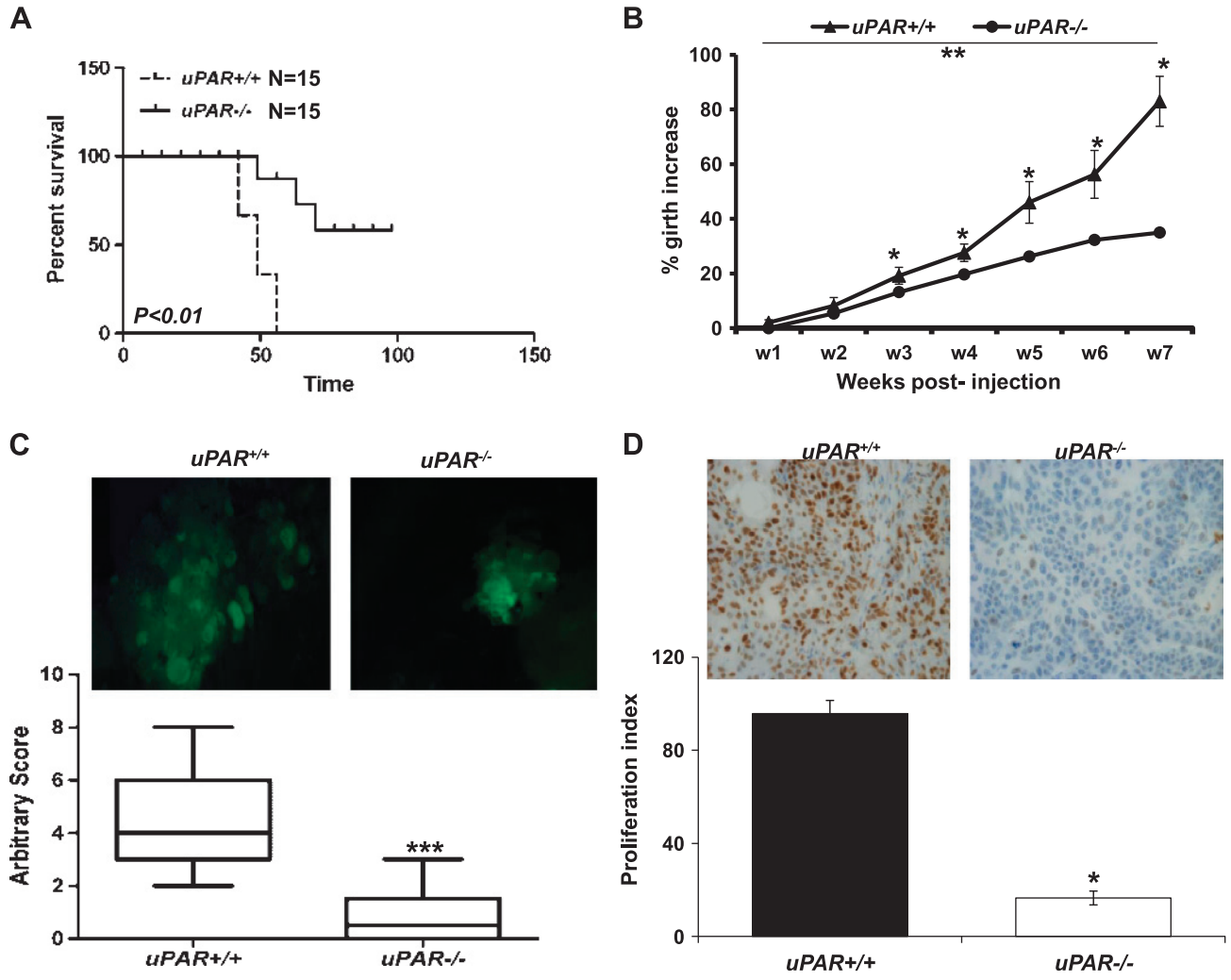

Figure 1. Effects of uPAR deficiency on ID8 intraperitoneal tumor growth. (A) Kaplan-Meier curve showing animal survival of *uPAR*$^{+/+}$ and *uPAR*$^{-/-}$ mice after IP injection of ID8-GFP cells (1×10^6 cells/500 μl PBS). (B) Tumor progression was monitored in the live animal by girth measurement for 7 weeks after injection of ID8 cells. *$P < .05$ between indicated time points in *uPAR*$^{+/+}$ and *uPAR*$^{-/-}$, Student's t test. **$P < .05$ in *uPAR*$^{+/+}$, one-way ANOVA. (C) Fluorescent photomicrographs (magnification, ×10) of representative IP tumor nodules developing in *uPAR*$^{+/+}$ and *uPAR*$^{-/-}$ (upper). Boxes (lower) represent mean ± SEM scores of peritoneal tumor nodules, and whiskers represent the minimum and maximum values. ***$P < .0001$, non–two-tailed parametric Mann-Whitney test. (D) Ki67 immunostaining of IP tumor nodules (magnification, ×200). Bars represent mean ± SEM of Ki67-positive nuclei counted in six random high-power fields (proliferation index). *$P < .001$, Student's t test.

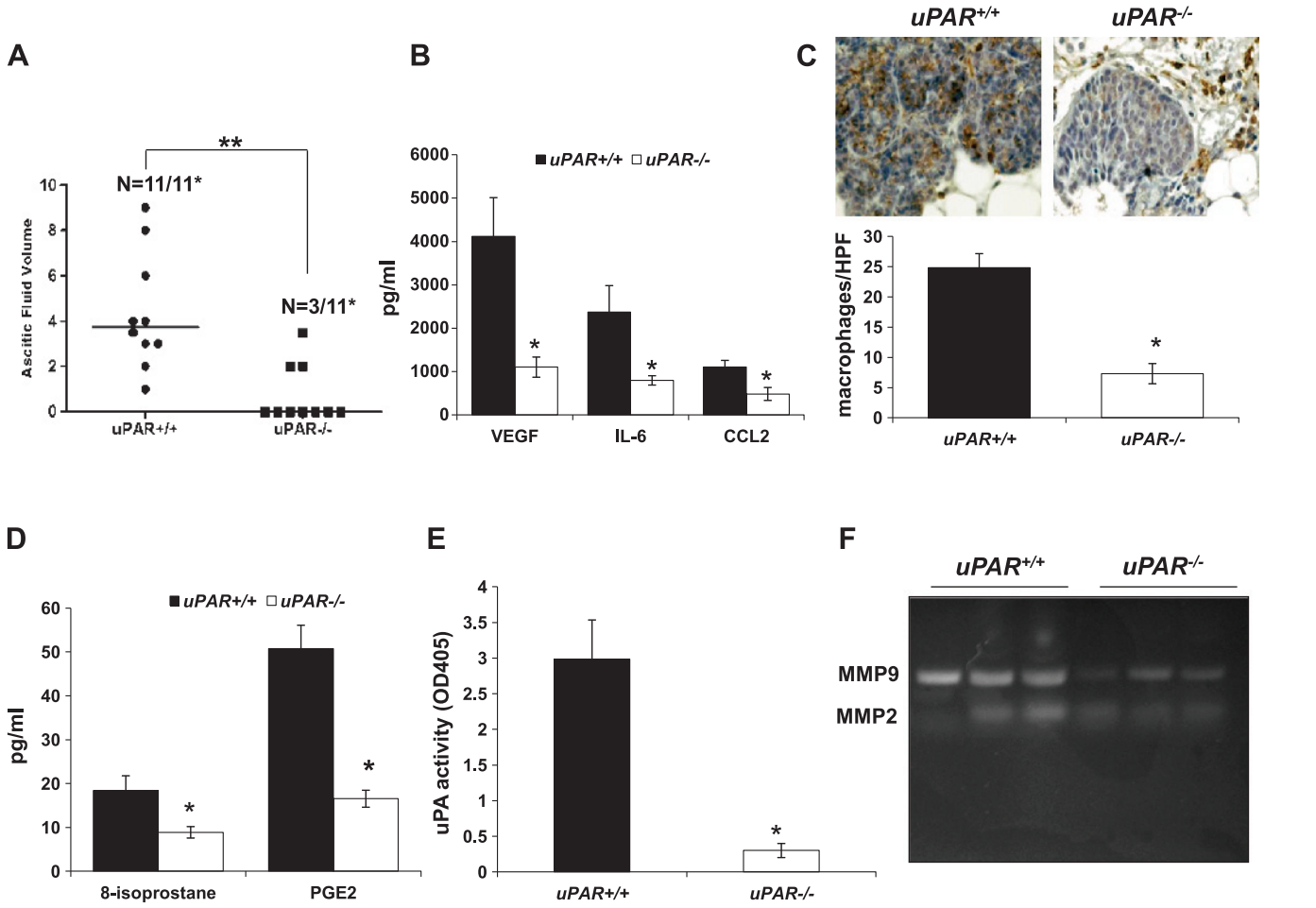

Figure 2. Absence of host uPAR is associated with decreased inflammation. (A) Scatterplots representing the incidence and volume of ascitic fluid measured in both genotypes at the end of 7 weeks after ID8 injection. Values represent mean ± SEM. *$P < .001$, comparing the incidence by χ^2 test. **$P < .05$, compared with the tumor volume in $uPAR^{-/-}$ mice. (B) Levels of VEGF, IL-6, and CCL2 in the ascitic fluid of $uPAR^{+/+}$ and $uPAR^{-/-}$ mice. (C) TAMs were determined by F4/80 immunostaining of $uPAR^{+/+}$ and $uPAR^{-/-}$ tumor tissues. Bars represent means ± SEM of macrophages counted in six high-power fields ($n = 3$ each; magnifications, ×200). *$P < .05$, Student's t test. (D) Levels of PGE_2 and 8-isoprostane were measured by enzyme immunoassay. (E) uPA activity in the ascetic fluid was determined as described in Materials and Methods. Bars represent means ± SEM of three representative experiments performed in triplicates. *$P < .05$, Student's t test. (F) Gelatin zymography of $uPAR^{+/+}$ and $uPAR^{-/-}$ ascitic fluids.

was slower in $uPAR^{-/-}$ mice as determined by measuring the girth of live mice (Figure 1*B*). To compensate for widespread dissemination of small tumor nodules in the peritoneal cavity and for the large tumor nodules whose margins are difficult to distinguish, we adopted two independent arbitrary scoring systems for each mouse considering the number and size of the visible tumor nodules, as earlier published [26] and described in the Materials and Methods. The average score/animal was calculated, and the means of the scores of animals in each cohort were calculated (Figure 1*C*). This approach provided adequate representation of the tumor burden. We also found that the number of proliferating cells was significantly decreased in tumors developing in $uPAR^{-/-}$ mice compared with their wild-types (Figure 1*D*). There was no difference in the distribution of metastatic lesions between $uPAR^{-/-}$ and their $uPAR^{+/+}$ counterparts. In the latter, tumor nodules not only grew on the mesothelium lining the peritoneal cavity but also broke through the mesothelial layer into the submesothelial stroma. Whereas in mice lacking uPAR, breaching the mesothelial layer and submesothelial invasion were observed only in one animal in which a few nodules broke through the mesothelial layer and invaded. It is noteworthy to mention that only mesenteric lymph nodes were involved in the $uPAR^{+/+}$ mice.

Host uPAR Contributes to Inflammatory Environment in POC

The incidence and volume of ascitic fluid accumulation were significantly lower in $uPAR^{-/-}$ mice (Figure 2*A*). It is noteworthy to mention that only two mice ascitic fluid volume correlated with the number and size of IP tumor implants. Lower levels of proinflammatory cytokines IL-6, CCL2, and VEGF (Figure 2*B*) were detected in $uPAR^{-/-}$ mice compared with their wild-type counterparts. Consistently, F4/80 immunostaining of tumor sections revealed that TAMs were significantly higher in wild-type compared with $uPAR^{-/-}$ mice (Figure 2*C*). In addition, significantly lower levels of PGE_2 and 8-isoprostane (Figure 2*D*) as well as uPA activity (Figure 2*E*) were detected in $uPAR^{-/-}$ ascitic fluid. Moreover, the enzymatic activity of MMP-2 and MMP-9 were lower in $uPAR^{-/-}$ ascitic fluid (Figure 2*F*). Together, these data indicate that the host uPAR suppresses tumor development of peritoneal ID8 tumor implants and decreases accumulation

malignant ascitic fluid concomitant with decreased infiltration of macrophages, inflammatory, and proteolytic activity.

Effect of uPAR on Ovarian Cancer Cell Interaction with Mesothelial Cells

We next sought to explain the effect of host uPAR on the development of IP ovarian tumors and to determine the contribution of the different cell types in the peritoneal microenvironment and their relevance to human disease. We and others [2,3,6,14,26,27,29,30,32,35] have reported that the first step in the development of POC is adhesion of the shed ovarian cancer cells to mesothelial cells lining the peritoneal cavity. In addition, we have earlier reported that coculture of ovarian cancer cells with mesothelial cells induces the expression and secretion of proinflammatory cytokines and mediators in the peritoneal milieu and in turn activates mesothelial cells to support further cancer cell adhesion [14,27,30]. To determine the role mesothelial uPAR in their interactions with cancer cells, we knocked down uPAR in human mesothelial cells and tested their ability to allow ovarian cancer cell adhesion. We found that knockdown of uPAR in mesothelial cells inhibited ovarian cancer cell adhesion (Figure 3*A*). We next determined

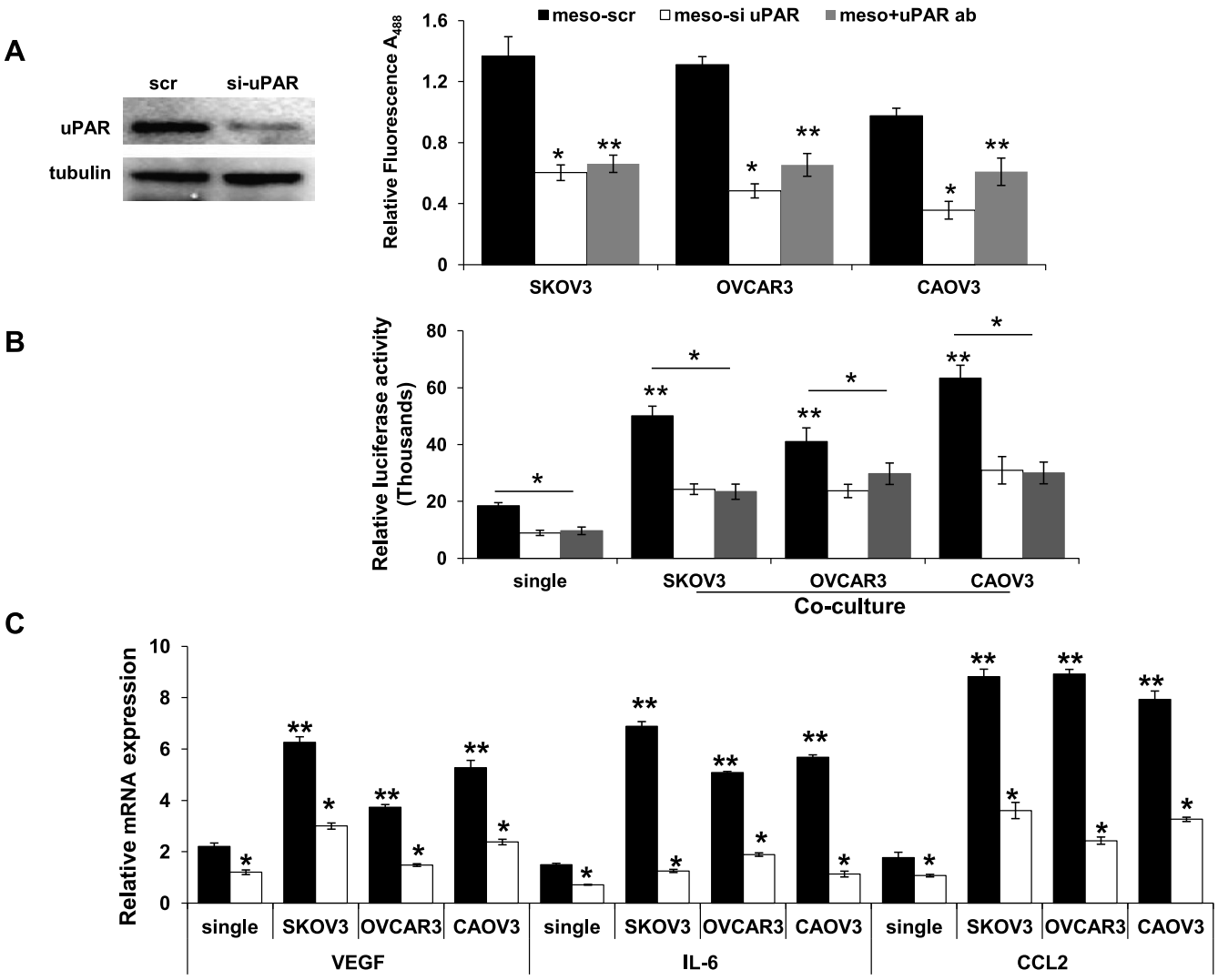

Figure 3. Effects of mesothelial uPAR on mesothelial-ovarian cancer cell interactions. (A) Western blot shows the effective knockdown of uPAR in Meso301 cell line and tubulin as a loading control. CMFDA-labeled UMUC3, OVCAR3, and CAOV3 were allowed to adhere to confluent monolayers of Meso301 depleted or not of uPAR expression by siRNA (si uPAR) or scrambled control (scr) in 24-well plates for 6 hours. In one set of experiments, mesothelial cells were treated with 10 μg/ml uPAR neutralizing antibody for 2 hours before and during incubation with cancer cells. After washing nonadherent cells, cancer cell adhesion was determined by measuring the fluorescent intensity at A_{488}. Bars represent the means ± SEM of three independent experiments performed in triplicates. *$P < .05$, between adhesion to scr and si uPAR Meso301. **$P < .05$ between scr and uPAR Ab-treated cells, Student's t test. (B) Meso301 cells were cotransfected with pNFκB luc, si uPAR, and scr siRNA 48 hours before coincubation with cancer cells or treatment with uPAR for a further 24 hours. NF-κB activation was determined by measuring the luciferase activity of cell lysates. Bars represent the means ± SEM of three independent experiments performed in triplicates. *$P < .05$, between Meso301scr cells and si uPAR or uPAR Ab in single culture or coculture. **$P < .05$ between Meso301 in single culture and coculture. (C) The levels of VEGF, IL-6, and CCL2 in Meso301 depleted or not of uPAR in single culture and coculture with ovarian cancer cells were determined by quantitative reverse transcription–polymerase chain reaction and were normalized to GAPDH. Bars represent the means ± SEM of normalized levels of three independent experiments performed in duplicates. *$P < .05$, between Meso301scr cells and si uPAR.

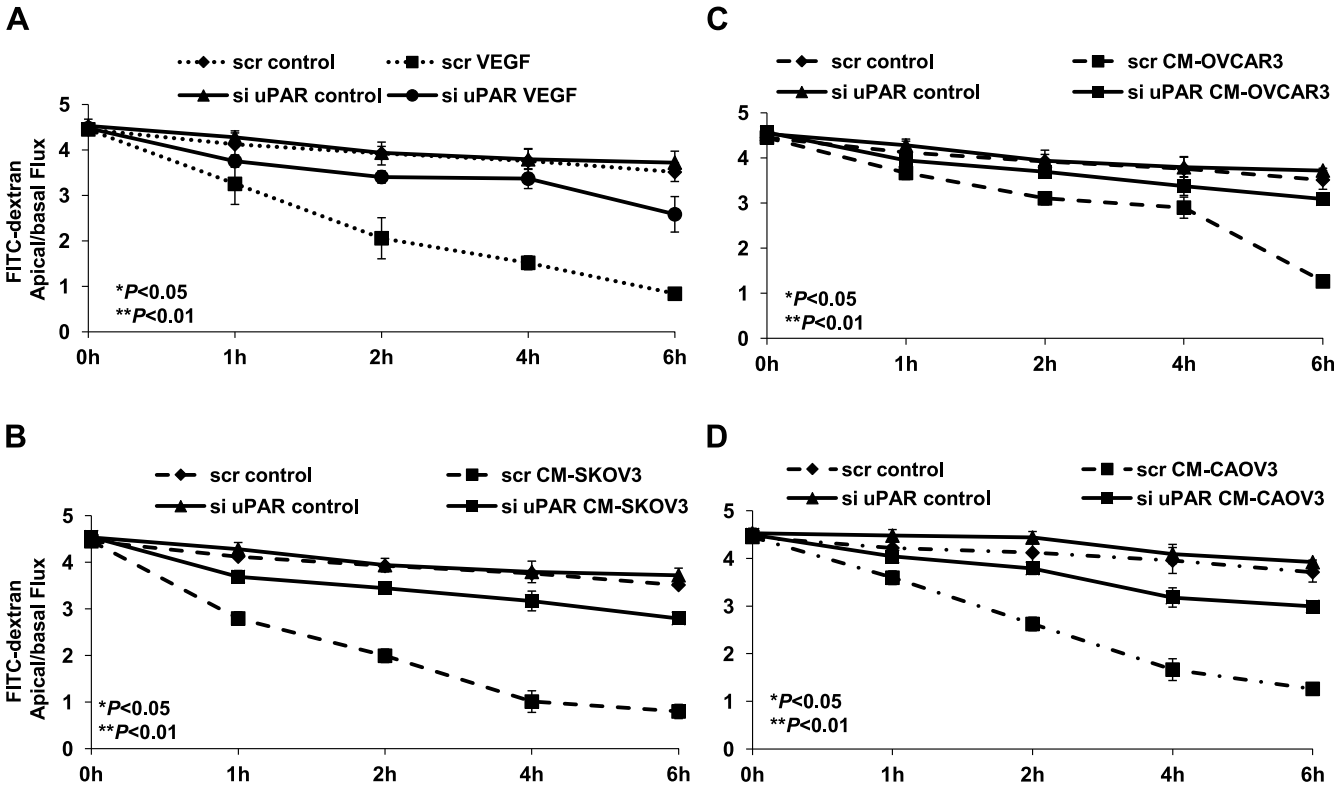

Figure 4. Effect of uPAR on vascular permeability. Confluent monolayers of HUVECs depleted or not of uPAR (scr and si-uPAR) were grown on transparent 0.4-μm filters for 48 hours and were apically treated with (A) VEGF (40 μg/ml) or 72-hour CM of (B) SKOV3, (C) OVCAR3, and (D) CAOV3 added apically on the top chamber of the transwells. The integrity of the endothelial barrier was determined by measuring the flux of FITC-dextran before and at the indicated times after treatment of HUVECs. Line graphs represent the mean ± SEM of the apical/basal fluorescence of the aliquots of collected from apical and basal chambers of the transwells. *$P < .05$, comparing the decrease in apical/basal flux in VEGF- or CM-treated scr control, one-way ANOVA. **$P < .01$, comparing the apical/basal flux between VEGF- or CM-treated scr control and si uPAR HUVECs, Student's *t* test.

whether adhesion of ovarian cancer cells to mesothelial cells triggers the activation of nuclear factor κB (NF-κB)—the key orchestrator of cancer-associated inflammation. We transfected mesothelial cells with NF-κB luciferase reporter after knockdown of uPAR and cocultured them with ovarian cancer cells for 24 hours. We found that knockdown of uPAR in mesothelial cells suppressed NF-κB activation in mesothelial cells whether they were cultured alone or cocultured with SKOV3, OVCAR3, and CAOV3 (Figure 3*B*). Furthermore, uPAR knockdown in mesothelial cells decreased the basal and coculture-induced up-regulation of inflammatory cytokines VEGF, IL-6, and CCL2 (Figure 3*C*) that have been shown to support ovarian cancer cell adhesion [14,30].

Effect of uPAR on Vascular Permeability

The increase in vascular permeability is a hallmark of ovarian cancer because it leads to the formation of extensive ascites in the earlier and later stages of the disease. Several studies have indicated that vascular endothelial growth factor (VEGF), also known as vascular permeability factor, is implicated in ascites formation, particularly in ovarian cancer [36,37]. Endothelial uPAR has been implicated in VEGF-mediated vascular permeability *in vitro* and *in vivo* [23,24,38]. Despite the recent reports of the effect of uPAR blockade by antibodies in ameliorating *in vivo* tumor growth of CAOV3 cells in nude mice [6], the effect of endothelial uPAR on vascular permeability and ascites formation is not elucidated. To determine whether endothelial cell uPAR affects their permeability, we knocked down uPAR in HUVECs and allowed them to grow to confluence on transwell filters. We tested the effect of VEGF (Figure 4*A*) and CM of SKOV3, OVCAR3, and CAOV3 ovarian cancer cell lines (Figure 4, *B-D*) on the paracellular flux of FITC-dextran through HUVECs monolayers. We found that VEGF-induced disruption of the endothelial tight junctions as determined by ZO-1 immunostaining of HUVECs monolayers was associated with increased FITC-dextran in the bottom chambers of the transwells and decreased apical/basal ratio and that this effect was mitigated by knocking down endothelial uPAR (Figure 5). Similar effects of FITC-dextran apical/basal flux were observed with CM of SKOV3, OVCAR3, and CAOV3 cells and were inhibited by the knockdown of endothelial uPAR. Treating HUVECs with anti–uPAR-neutralizing antibody had partially antagonized the permeability-inducing effect of VEGF and CM of ovarian cancer cells (Figure W1). To determine the *in vivo* specificity of uPAR and VEGF interactions, we injected ID8 cells stably expressing VEGF [25,27] IP in $uPAR^{+/+}$ and $uPAR^{-/-}$ mice and monitored tumor progression as described above. We found that, despite constitutive overexpression of VEGF in ID8 cells, the accumulation of ascitic fluid in $uPAR^{-/-}$ mice was significantly lower than that in $uPAR^{+/+}$, concomitant with slower disease progression and longer median animal survival (Figure W2).

Genetic Ablation and Neutralization of Macrophage uPAR Inhibited Their In Vitro *Interactions with Cancer Cells*

TAMs have been shown to contribute to the inflammatory microenvironment in ovarian cancer and were associated with poor prognosis [35,39,40]. We and others have previously shown that macrophages increase the invasive phenotype of ovarian cancer cells and contribute to augmented production of inflammatory mediators *in vitro* and *in vivo*. In addition, macrophages contributed to increased proteolytic activity of MMP-2 and MMP-9 as well as uPA activity when cocultured of ovarian cancer cells [14,26,27,29,30,39–41]. Furthermore, impaired growth of prostate cancer cells in $uPAR^{-/-}$ and $uPA^{-/-}$ mice was associated with decreased macrophage infiltration and decreased cancer cell invasiveness [8]. To further investigate the roles of the uPA/uPAR axis in macrophage chemotaxis *in vitro*, we found that depletion of uPAR in human U937 macrophages suppressed their ability to migrate toward CM from SKOV3, CAOV3, and OVCAR3 cells (Figure 6*A*). Consistently, uPAR-depleted U937 cells exhibited decreased ability to induce SKOV3, CAOV3, and OVCAR3 cells' invasiveness (Figure 6*B*). Similar effect was noticed by neutralization of uPAR by a neutralizing antibody (Figure 6*C*). We next determined whether macrophage uPAR is involved in the activation of NF-κB induced by their coculture with ovarian cancer cells, we transfected U937 cells with NF-κB luciferase reporter after knockdown of uPAR and cocultured them with ovarian cancer cells for 24 hours and found that knockdown of uPAR in U937 cells suppressed NF-κB activation whether they were cultured alone or cocultured with SKOV3, OVCAR3, and CAOV3 (Figure 6*D*).

Expression of uPAR in Human Ovarian Tumors

Previous studies have reported various expression levels of uPAR in ovarian cancer (summarized in Kenny et al. [6]). In their comprehensive study, Kenny et al. [6] reported the expression of uPAR in 92% of patients with ovarian cancer with a stronger expression in the cancerous epithelium than the stroma and absent or low in normal ovarian surface epithelium. Although uPAR expression was found to be independent of the classic clinicopathologic parameters, platinum sensitivity, or patients' survival, they reported they reported the efficiency of blocking uPAR in inhibiting ovarian cancer cell adhesion and invasion *in vitro* and *in vivo*. Together with the earlier reports that uPAR is elevated in tumors, serum, and ascitic fluid as well as our *in vivo* and *in vitro* findings, we sought to analyze uPAR expression in human ovarian tumors taking into account the tumor heterogeneity, stromal uPAR, as well as the different grades. We adopted a scoring system that combined the intensity and the frequency of staining and allowed to distinguish stromal from tumor uPAR (Figure 7*A*). In accord with earlier reports [6], we found lower levels of uPAR in normal ovarian tissues, both epithelium and stroma. The hypothesis is that the probability of the increase in the level of uPAR in early tumor stages precedes the increase in intensity and frequency of distribution in tumors. The

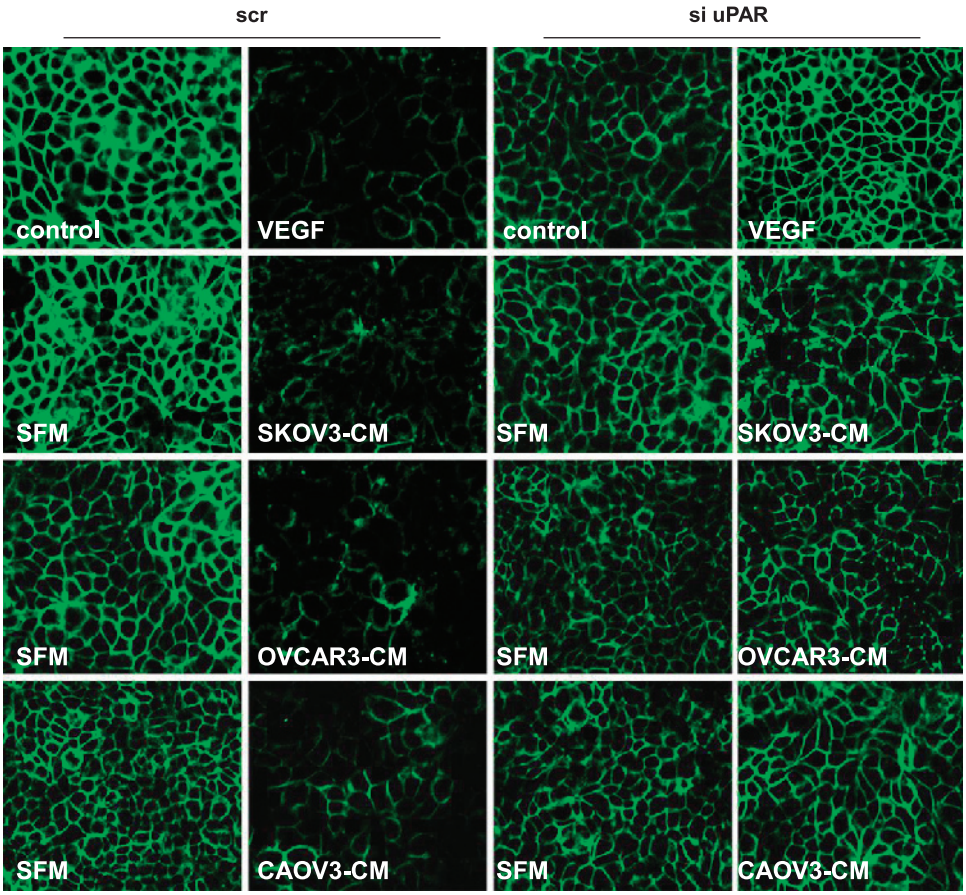

Figure 5. Effect of uPAR of endothelial tight junctions. Confluent monolayers of HUVECs were grown and treated as described in Figure 4. At the end of 6 hours, filters were fixed and immunostained for ZO-1, mounted in fluorescence mounting medium, and were analyzed by fluorescence microscopy. Total magnification, ×400. Images are representative of at three filters/each condition.

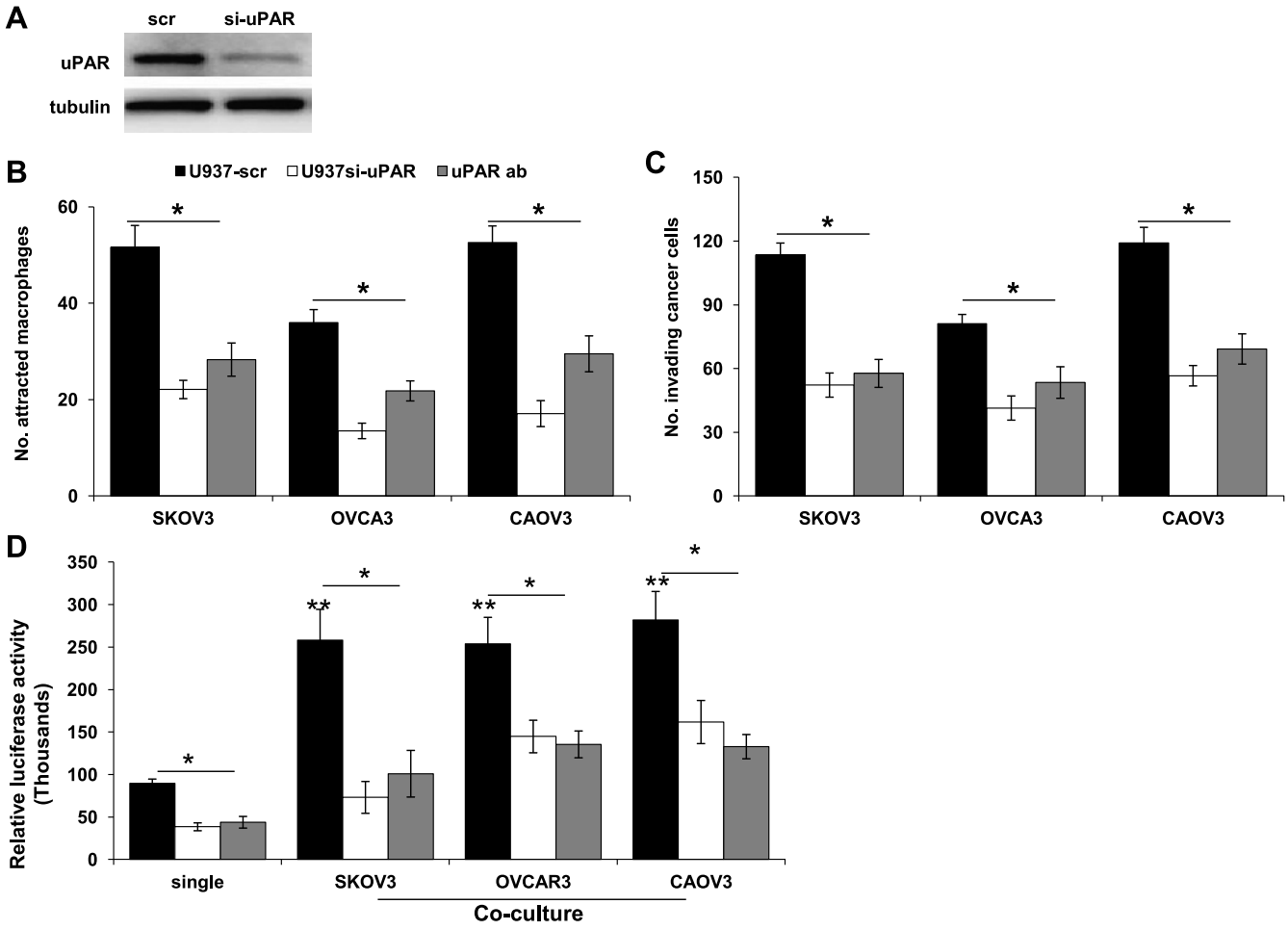

Figure 6. Effects of uPAR deficiency on macrophage chemotaxis. (A) Western blot shows the effective knockdown of uPAR in U937 macrophages with tubulin as a loading control. (B) *In vitro* chemotaxis assays of U937 cells depleted or not of uPAR through Matrigel-coated 3-μm filters toward 72-hour CM of SKOV3, OVCAR3, and CAOV3 cells as described in Materials and Methods. (C) SKOV3, OVCAR3, and OVCAR3 were allowed to invade Matrigel-coated 8-μm inserts toward CM from U937-scr and U937-si uPAR for 5 hours. As a control, a blocking uPAR Ab (10 μg/ml) was used. Bars represent mean ± SEM of counted invading/attracted cells of three independent experiments performed in triplicates. *$P < .01$, compared with control scr-U937 cells, Student's *t* test. (D) U937 cells were cotransfected with pNFκB luc, si uPAR, and scr siRNA 48 hours before coculture with subconfluent monolayers of ovarian cancer cells grown in 24 wells. U937 (1×10^6) cells were added on 0.4-μm filters without cell-cell contact or treatment with uPAR for further 24 hours. NF-κB activation was determined by measuring the luciferase activity of cell lysates. Bars represent the means ± SEM of three independent experiments performed in triplicates. *$P < .05$, between U937- scr cells and si uPAR or uPAR Ab in single culture and coculture. **$P < .05$, between U937 cells in single culture and coculture.

expression levels of uPAR were significantly higher in cancerous epithelium (Figure 7*B*), and juxtatumoral stroma (Figure 7*C*). Comparing uPAR tumor and stromal composite expression scores between normal and each grade was significant when analyzed by Kruskal-Wallis test and receiver operating characteristic curve. In addition, when comparing, the tumor grades were significant when analyzed by Kruskal-Wallis test and the Dunn post hoc test; the correlation between uPAR scores among different grades was insignificant.

Together, these data indicate that the utility of uPAR as a prognostic marker in ovarian cancer may vary among the different studies owing to technical analytical variables.

Discussion

uPAR has been reported as a tumor promoter in several solid cancers through a mitogenic, proinvasive effect on cancer cells [6,7,11,22,42,43]. In addition, genetic manipulation of uPAR in tumor cells or functional neutralization by neutralizing antibodies demonstrated its importance as a therapeutic target [6,7,11,22,42,43]. However, to date, the mechanistic role of host uPAR in ovarian cancer progression and development of peritoneal implants and malignant ascitic fluid has not been shown. In addition, because uPAR can be produced by both the tumor and the host, the contributions of each of these compartments to ovarian cancer progression have not been defined. However, the contribution of host-derived uPAR on ovarian cancer development and development of recalcitrant recurrent disease remains unclear.

In the current study, we systematically demonstrated the role of host uPAR in ovarian cancer. Using a syngeneic ovarian cancer model in $uPAR^{+/+}$ and $uPAR^{-/-}$ mice, we found that tumor take, growth, progression, and median animal survival were dramatically diminished in $uPAR^{-/-}$ mice compared with $uPAR^{+/+}$ controls. Consistently, we found decreased proliferation of tumor cells in $uPAR^{-/-}$ mice compared with their $uPAR^{+/+}$. This was expected because of the impairment of

survival signaling cascades activated by the interaction of uPAR with integrins, growth factor receptors, and ECM molecules [6,7,11, 22,42,43], which has been shown to be crucial for ovarian cancer progression (reviewed in Lengyel [2] and Kenny et al. [6]).

In addition, tumors in *uPAR*$^{-/-}$ mice displayed significantly less infiltrating TAMs, ascitic fluid volume, as well as the levels of VEGF, CCL2, and IL-6 in the ascitic fluid. These three factors, in particular, have been linked to the aggressiveness of the human ovarian cancer as well as the recurrence and chemoresistance, with accumulation of large volumes of ascitic fluid [2,12,13,44–47]. In addition to its putative potent angiogenic function, VEGF is also responsible for vascular permeability and formation of malignant ascites [36,37,48]. Similarly, the proinflammatory cytokines IL-6 and CCL2 are not only implicated in recruitment and activation of TAM but also are shown to exert potent mitogenic, proinvasive, and angiogenic effects in many cancers including ovarian cancer [12,14,27,30,31,40,42,46,47]. Furthermore, IL-6 and CCL2 were implicated in disruption or epithelial and endothelial barriers in microvascular and pulmonary diseases [49,50]. Moreover, the decreased levels of PGE_2 and 8-isoprostane together with decreased proteolytic activity of uPA, MMP-2, and MMP-9 in *uPAR*$^{-/-}$ mice compared with their *uPAR*$^{+/+}$ controls further explain the decreased *in vivo* tumor growth and accumulation of ascitic fluid. Interestingly, these factors are downstream of as well as activators of NF-κB—the key orchestrator of inflammation and ovarian cancer progression [13,44].

Our *in vivo* and *in vitro* findings reveal that knockdown of uPAR in mesothelial cells did not support SKOV3, OVCAR3, and CAOV3 cell adhesion, suggesting impaired interactions of uPAR, with integrins and ECM proteins such as vitronectin, fibronectin, and laminin 5 that are overexpressed in invasive cancer cells [51–54]. In addition, depletion of uPAR in mesothelial cells attenuated their basal and cancer cell–induced NF-κB activation with a subsequent decrease in coculture-induced VEGF, IL-6, and CCL2 levels that are implicated not only in chemotaxis of tumor cells toward mesothelial cells but also in survival, adhesion, invasiveness, and angiogenesis [14,27,30,31,52].

Herein, we also provide evidence that endothelial uPAR plays an important role in the accumulation of ascitic fluid. We show that depletion of endothelial uPAR mitigates the permeability-inducing effect of VEGF as well as that of CM of ovarian cancer cells and that it was mediated, in part, through maintaining the integrity of the tight junction protein ZO-1. The antagonistic effect of uPAR on VEGF-induced vascular permeability was further supported *in vivo* by decreased accumulation of ascitic fluid in *uPAR*$^{-/-}$ injected with ID8 cells stably overexpressing VEGF compared with accumulation in *uPAR*$^{+/+}$. These observations may provide an explanation of the increased levels of serum and ascitic fluid uPAR in patients with advanced ovarian cancer [52,55–58].

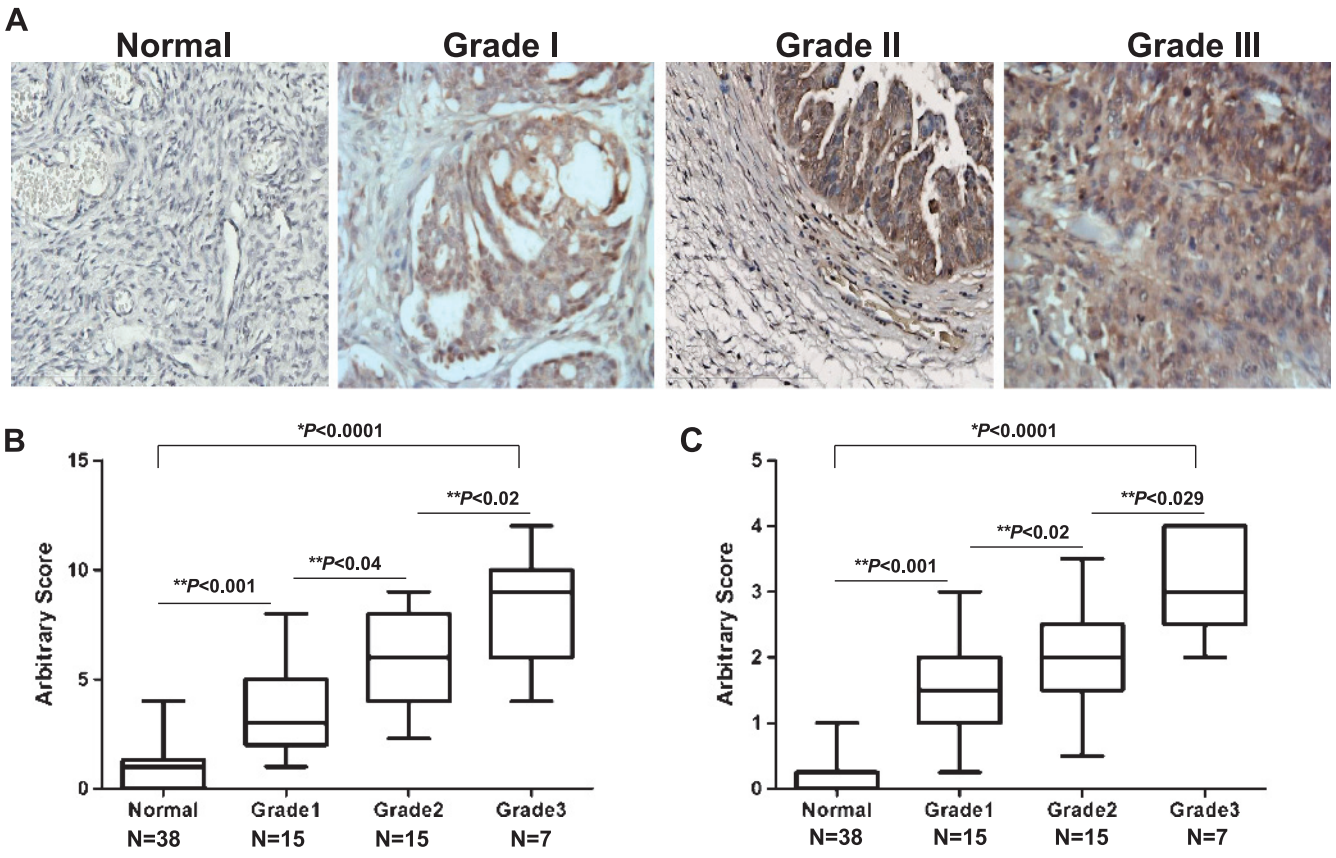

Figure 7. uPAR expression in normal and cancerous ovarian tissues. (A) Immunostaining of uPAR in human ovarian cancer and normal ovarian tissues TMAs (magnification, ×200). (B and C) The two arbitrary scores for intensity and frequency of uPAR immunostaining in the indicated groups of tumor (B) and stromal (C) compartments and normal tissues were transformed into composite expression scores as described in the Materials and Methods. Boxes represent the mean ± SEM with whiskers minimum and maximum scores for each group. *Correlation of composite scores in association with tumor grades by one-way ANOVA. **Correlation of composite scores between indicated groups by one-way ANOVA with Bonferroni multiple comparison test and receiver operating characteristic curve.

Furthermore, genetic ablation of macrophage uPAR impaired macrophage recruitment to the developing *in vivo* tumors (TAM), their ability to migrate toward CM of cancer cells, as well as the ability of their secretome to induce cancer cell invasiveness *in vitro* [15]—a process that involves activation of NF-κB in macrophages [52] with smoldering cancer inflammation and progression.

In conclusion, our results showed that host uPAR augments ovarian cancer cell proliferation, mesothelial adhesion, and invasiveness. Moreover, mesothelial and macrophage uPARs modulate their interactions with cancer cells. These results suggest a novel mechanism for the regulation of uPAR-induced cellular functions that may extend its therapeutic targeting in ovarian cancer to minimize the toxicity of standard-of-care therapies. Given the limited and often controversial effects of VEGF-based therapies, targeting uPAR as a downstream effector of VEGF-induced vascular permeability may provide beneficial advantage to inhibit the formation of ascites.

References

[1] Jemal A, Bray F, Center MM, Ferlay J, Ward E, and Forman D (2011). Global cancer statistics. *CA Cancer J Clin* **61**, 69–90.

[2] Lengyel E (2010). Ovarian cancer development and metastasis. *Am J Pathol* **177**, 1053–1064.

[3] Kenny HA, Nieman KM, Mitra AK, and Lengyel E (2011). The first line of abdominal metastatic attack: breaching the mesothelial cell layer. *Cancer Discov* **1**, 100–102.

[4] Iwanicki MP, Davidowitz RA, Ng MR, Besser A, Muranen T, Merritt M, Danuser G, Ince T, and Brugge JS (2011). Ovarian cancer spheroids use myosin-generated force to clear the mesothelium. *Cancer Discov* **1**, 144–157.

[5] Vassalli JD, Baccino D, and Belin D (1985). A cellular binding site for the M_r 55,000 form of the human plasminogen activator, urokinase. *J Cell Biol* **100**, 86–92.

[6] Kenny HA, Leonhardt P, Ladanyi A, Yamada SD, Montag A, Im HK, Jagadeeswaran S, Shaw DE, Mazar AP, and Lengyel E (2011). Targeting the urokinase plasminogen activator receptor inhibits ovarian cancer metastasis. *Clin Cancer Res* **17**, 459–471.

[7] Mazar AP (2008). Urokinase plasminogen activator receptor choreographs multiple ligand interactions: implications for tumor progression and therapy. *Clin Cancer Res* **14**, 5649–5655.

[8] Zhang J, Sud S, Mizutani K, Gyetko MR, and Pienta KJ (2011). Activation of urokinase plasminogen activator and its receptor axis is essential for macrophage infiltration in a prostate cancer mouse model. *Neoplasia* **13**, 23–30.

[9] Jo M, Thomas KS, Takimoto S, Gaultier A, Hsieh EH, Lester RD, and Gonias SL (2007). Urokinase receptor primes cells to proliferate in response to epidermal growth factor. *Oncogene* **26**, 2585–2594.

[10] Lester RD, Jo M, Montel V, Takimoto S, and Gonias SL (2007). uPAR induces epithelial-mesenchymal transition in hypoxic breast cancer cells. *J Cell Biol* **178**, 425–436.

[11] Choong PF and Nadesapillai AP (2003). Urokinase plasminogen activator system: a multifunctional role in tumor progression and metastasis. *Clin Orthop Relat Res* **(415 suppl)**, S46–S58.

[12] Kohn EC, Travers LA, Kassis J, Broome U, and Klominek J (2005). Malignant effusions are sources of fibronectin and other promigratory and proinvasive components. *Diagn Cytopathol* **33**, 300–308.

[13] Hernandez L, Hsu SC, Davidson B, Birrer MJ, Kohn EC, and Annunziata CM (2010). Activation of NF-κB signaling by inhibitor of NF-κB kinase β increases aggressiveness of ovarian cancer. *Cancer Res* **70**, 4005–4014.

[14] Said NA, Elmarakby AA, Imig JD, Fulton DJ, and Motamed K (2008). SPARC ameliorates ovarian cancer–associated inflammation. *Neoplasia* **10**, 1092–1104.

[15] Saito Y, Sekine W, Sano R, Komatsu S, Mizuno H, Katabami K, Shimada K, Oku T, and Tsuji T (2010). Potentiation of cell invasion and matrix metalloproteinase production by $\alpha_3\beta_1$ integrin–mediated adhesion of gastric carcinoma cells to laminin-5. *Clin Exp Metastasis* **27**, 197–205.

[16] Estreicher A, Mühlhauser J, Carpentier JL, Orci L, and Vassalli JD (1990). The receptor for urokinase type plasminogen activator polarizes expression of the protease to the leading edge of migrating monocytes and promotes degradation of enzyme inhibitor complexes. *J Cell Biol* **111**, 783–792.

[17] Gyetko MR, Todd RF, Wilkinson CC, and Sitrin RG (1994). The urokinase receptor is required for human monocyte chemotaxis *in vitro*. *J Clin Invest* **93**, 1380–1387.

[18] Busso N, Masur SK, Lazega D, Waxman S, and Ossowski L (1994). Induction of cell migration by pro-urokinase binding to its receptor: possible mechanism for signal transduction in human epithelial cells. *J Cell Biol* **126**, 259–270.

[19] Alexander RA, Prager GW, Mihaly-Bison J, Uhrin P, Sunzenauer S, Binder BR, Schutz GJ, Freissmuth M, and Breuss JM (2012). VEGF-induced endothelial cell migration requires urokinase receptor (uPAR)–dependent integrin redistribution. *Cardiovasc Res* **94**, 125–135.

[20] Balsara RD, Merryman R, Virjee F, Northway C, Castellino FJ, and Ploplis VA (2011). A deficiency of uPAR alters endothelial angiogenic function and cell morphology. *Vasc Cell* **3**, 10.

[21] Prager GW, Breuss JM, Steurer S, Mihaly J, and Binder BR (2004). Vascular endothelial growth factor (VEGF) induces rapid prourokinase (pro-uPA) activation on the surface of endothelial cells. *Blood* **103**, 955–962.

[22] Malla RR, Gopinath S, Gondi CS, Alapati K, Dinh DH, Gujrati M, and Rao JS (2011). Cathepsin B and uPAR knockdown inhibits tumor-induced angiogenesis by modulating VEGF expression in glioma. *Cancer Gene Ther* **18**, 419–434.

[23] Behzadian MA, Windsor LJ, Ghaly N, Liou G, Tsai NT, and Caldwell RB (2003). VEGF-induced paracellular permeability in cultured endothelial cells involves urokinase and its receptor. *FASEB J* **17**, 752–754.

[24] El-Remessy AB, Behzadian MA, Abou-Mohamed G, Franklin T, Caldwell RW, and Caldwell RB (2003). Experimental diabetes causes breakdown of the blood-retina barrier by a mechanism involving tyrosine nitration and increases in expression of vascular endothelial growth factor and urokinase plasminogen activator receptor. *Am J Pathol* **162**, 1995–2004.

[25] Zhang L, Yang N, Garcia JR, Mohamed A, Benencia F, Rubin SC, Allman D, and Coukos G (2002). Generation of a syngeneic mouse model to study the effects of vascular endothelial growth factor in ovarian carcinoma. *Am J Pathol* **161**, 2295–2309.

[26] Said N and Motamed K (2005). Absence of host-secreted protein acidic and rich in cysteine (SPARC) augments peritoneal ovarian carcinomatosis. *Am J Pathol* **167**, 1739–1752.

[27] Said N, Socha MJ, Olearczyk JJ, Elmarakby AA, Imig JD, and Motamed K (2007). Normalization of the ovarian cancer microenvironment by SPARC. *Mol Cancer Res* **5**, 1015–1030.

[28] Bugge TH, Suh TT, Flick MJ, Daugherty CC, Rømer J, Solberg H, Ellis V, Danø K, and Degen JL (1995). The receptor for urokinase-type plasminogen activator is not essential for mouse development or fertility. *J Biol Chem* **270**, 16886–16894.

[29] Said N, Najwer I, and Motamed K (2007). Secreted protein acidic and rich in cysteine (SPARC) inhibits integrin-mediated adhesion and growth factor–dependent survival signaling in ovarian cancer. *Am J Pathol* **170**, 1054–1063.

[30] Said NA, Najwer I, Socha MJ, Fulton DJ, Mok SC, and Motamed K (2007). SPARC inhibits LPA-mediated mesothelial-ovarian cancer cell crosstalk. *Neoplasia* **9**, 23–35.

[31] Said N, Frierson HF Jr, Chernauskas D, Conaway M, Motamed K, and Theodorescu D (2009). The role of SPARC in the TRAMP model of prostate carcinogenesis and progression. *Oncogene* **28**, 3487–3498.

[32] Said N, Smith S, Sanchez-Carbayo M, and Theodorescu D (2011). Tumor endothelin-1 enhances metastatic colonization of the lung in mouse xenograft models of bladder cancer. *J Clin Invest* **121**, 132–147.

[33] Coyne CB, Ribeiro CM, Boucher RC, and Johnson LG (2003). Acute mechanism of medium chain fatty acid–induced enhancement of airway epithelial permeability. *J Pharmacol Exp Ther* **305**, 440–450.

[34] Coyne CB, Vanhook MK, Gambling TM, Carson JL, Boucher RC, and Johnson LG (2002). Regulation of airway tight junctions by proinflammatory cytokines. *Mol Biol Cell* **13**, 3218–3234.

[35] Davidson B, Reich R, Kopolovic J, Berner A, Nesland JM, Kristensen GB, Trope CG, Bryne M, Risberg B, van de Putte G, et al. (2002). Interleukin-8 - and vascular endothelial growth factor mRNA and protein levels are down-regulated in ovarian carcinoma cells in serous effusions. *Clin Exp Metastasis* **19**, 135–144.

[36] Nagy JA, Masse EM, Herzberg KT, Meyers MS, Yeo K-T, Yeo T-K, Sioussat TM, and Dvorak HF (1995). Pathogenesis of ascites tumor growth: vascular permeability factor, vascular hyperpermeability, and ascites fluid accumulation. *Cancer Res* **55**, 360–368.

[37] Hu L, Ferrara N, and Jaffe RB (2006). Paracrine VEGF/VE-cadherin action on ovarian cancer permeability. *Exp Biol Med* **231**, 1646–1652.

[38] Yang J, Duh EJ, Caldwell RB, and Behzadian MA (2010). Antipermeability function of PEDF involves blockade of the MAP kinase/GSK/β-catenin signaling pathway and uPAR expression. *Invest Ophthalmol Vis Sci* **51**, 3273–3280.

[39] Duluc D, Delneste Y, Tan F, Moles MP, Grimaud L, Lenoir J, Preisser L, Anegon I, Catala L, Ifrah N, et al. (2007). Tumor-associated leukemia inhibitory factor and IL-6 skew monocyte differentiation into tumor-associated macrophage-like cells. *Blood* **110**, 4319–4330.

[40] Hagemann T, Wilson J, Burke F, Kulbe H, Li NF, Pluddemann A, Charles K, Gordon S, and Balkwill FR (2006). Ovarian cancer cells polarize macrophages toward a tumor-associated phenotype. *J Immunol* **176**, 5023–5032.

[41] Fang J, Wei WN, Xia LH, and Song SJ (2004). Study of the effect of TF/FVIIa complex on the expression of u-PAR mRNA in human ovarian cancer [in Chinese]. *Zhonghua Xue Ye Xue Za Zhi* **25**, 143–146.

[42] Nalla AK, Gogineni VR, Gupta R, Dinh DH, and Rao JS (2011). Suppression of uPA and uPAR blocks radiation-induced MCP-1 mediated recruitment of endothelial cells in meningioma. *Cell Signal* **23**, 1299–1310.

[43] Raghu H, Nalla AK, Gondi CS, Gujrati M, Dinh DH, and Rao JS (2012). uPA and uPAR shRNA inhibit angiogenesis via enhanced secretion of SVEGFR1 independent of GM-CSF but dependent on TIMP-1 in endothelial and glioblastoma cells. *Mol Oncol* **6**, 33–47.

[44] Chechlinska M, Kaminska J, Markowska J, Kramar A, and Steffen J (2007). Peritoneal fluid cytokines and the differential diagnosis of benign and malignant ovarian tumors and residual/recurrent disease examination. *Int J Biol Markers* **22**, 172–180.

[45] Chen SS, Michael A, and Butler-Manuel SA (2012). Advances in the treatment of ovarian cancer—a potential role of antiinflammatory phytochemicals. *Discov Med* **13**, 7–17.

[46] Coward J, Kulbe H, Chakravarty P, Leader D, Vassileva V, Leinster DA, Thompson R, Schioppa T, Nemeth J, Vermeulen J, et al. (2011). Interleukin-6 as a therapeutic target in human ovarian cancer. *Clin Cancer Res* **17**, 6083–6096.

[47] Giuntoli RL II, Webb TJ, Zoso A, Rogers O, Diaz-Montes TP, Bristow RE, and Oelke M (2009). Ovarian cancer–associated ascites demonstrates altered immune environment: implications for antitumor immunity. *Anticancer Res* **29**, 2875–2884.

[48] Akutagawa N, Nishikawa A, Iwasaki M, Fujimoto T, Teramoto M, Kitajima Y, Endo T, Shibuya M, and Kudo R (2002). Expression of vascular endothelial growth factor and E-cadherin in human ovarian cancer: association with ascites fluid accumulation and peritoneal dissemination in mouse ascites model. *Jpn J Cancer Res* **93**, 644–651.

[49] Brown CM, Mulcahey TA, Filipek NC, and Wise PM (2010). Production of proinflammatory cytokines and chemokines during neuroinflammation: novel roles for estrogen receptors α and β. *Endocrinology* **151**, 4916–4925.

[50] Funatsu H, Noma H, Mimura T, Eguchi S, and Hori S (2009). Association of vitreous inflammatory factors with diabetic macular edema. *Ophthalmology* **116**, 73–79.

[51] Ahmed N, Riley C, Oliva K, Rice G, and Quinn M (2005). Ascites induces modulation of $\alpha_6\beta_1$ integrin and urokinase plasminogen activator receptor expression and associated functions in ovarian carcinoma. *Br J Cancer* **92**, 1475–1485.

[52] Kobayashi H, Yagyu T, Kondo T, Kurita N, Inagaki K, Haruta S, Kawaguchi R, Kitanaka T, Sakamoto Y, Yamada Y, et al. (2005). Suppression of urokinase receptor expression by thalidomide is associated with inhibition of nuclear factor κB activation and subsequently suppressed ovarian cancer dissemination. *Cancer Res* **65**, 10464–10471.

[53] Mekkawy AH, De Bock CE, Lin Z, Morris DL, Wang Y, and Pourgholami MH (2010). Novel protein interactors of urokinase-type plasminogen activator receptor. *Biochem Biophys Res Commun* **399**, 738–743.

[54] Mekkawy AH, Morris DL, and Pourgholami MH (2012). HAX1 augments cell proliferation, migration, adhesion, and invasion induced by urokinase-type plasminogen activator receptor. *J Oncol* **2012**, 950749.

[55] Begum FD, Hogdall CK, Kjaer SK, Christensen L, Blaakaer J, Bock JE, Glud E, Hoyer-Hansen G, Ring-Larsen H, and Hogdall EV (2004). The prognostic value of plasma soluble urokinase plasminogen activator receptor (suPAR) levels in stage III ovarian cancer patients. *Anticancer Res* **24**, 1981–1985.

[56] Chambers SK, Gertz RE Jr, Ivins CM, and Kacinski BM (1995). The significance of urokinase-type plasminogen activator, its inhibitors, and its receptor in ascites of patients with epithelial ovarian cancer. *Cancer* **75**, 1627–1633.

[57] Sier CF, Nicoletti I, Santovito ML, Frandsen T, Aletti G, Ferrari A, Lissoni A, Giavazzi R, Blasi F, and Sidenius N (2004). Metabolism of tumour-derived urokinase receptor and receptor fragments in cancer patients and xenografted mice. *Thromb Haemost* **91**, 403–411.

[58] Sier CF, Stephens R, Bizik J, Mariani A, Bassan M, Pedersen N, Frigerio L, Ferrari A, Dano K, Brunner N, et al. (1998). The level of urokinase-type plasminogen activator receptor is increased in serum of ovarian cancer patients. *Cancer Res* **58**, 1843–1849.

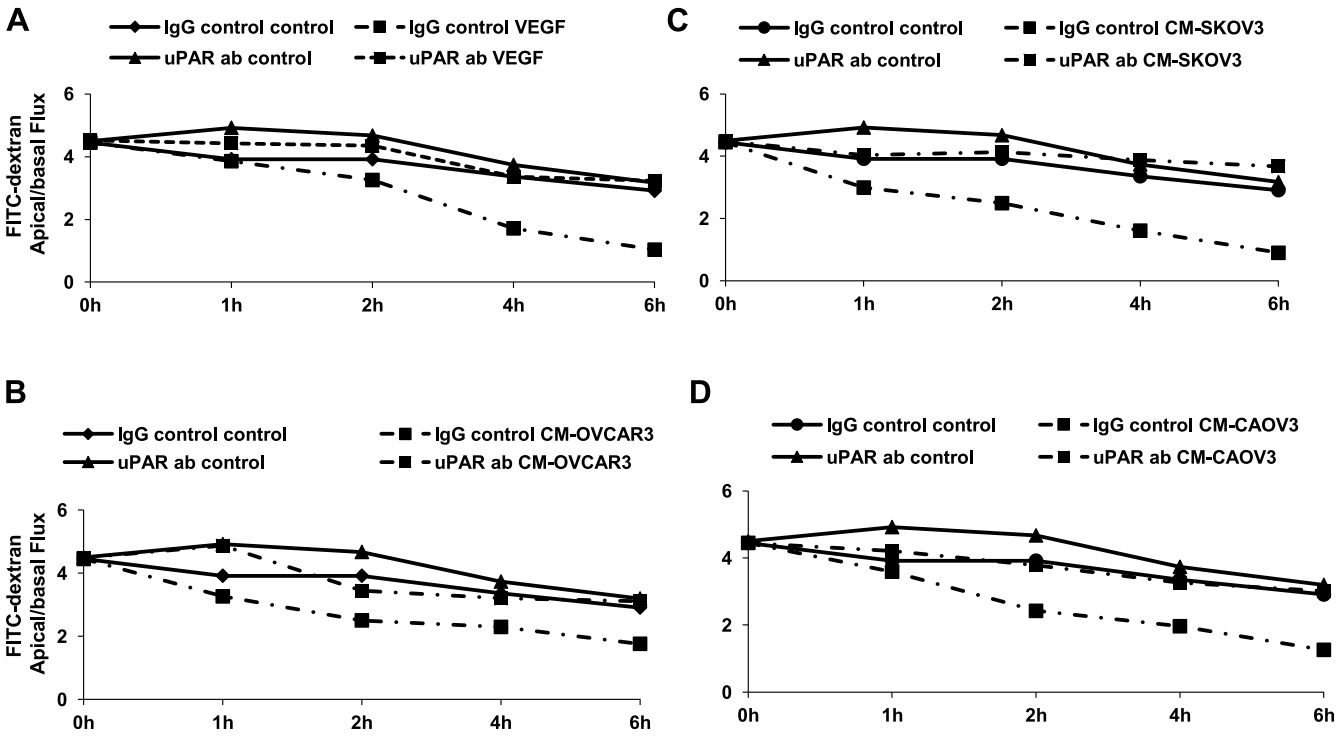

Figure W1. Neutralization of uPAR inhibits vascular permeability. Confluent monolayers of HUVECs were grown on transparent 0.4-μm filters for 48 hours and were pretreated with 10 μg/ml anti–uPAR-neutralizing antibody or isotype IgG control for an hour before apical treatment with (A) VEGF (40 μg/ml) or 72-hour CM of (B) SKOV3, (C) OVCAR3, and (D) CAOV3 added apically on the top chamber of the transwells. The integrity of the endothelial barrier was determined by measuring the flux of FITC-dextran before and at the indicated times after treatment of HUVECs. Line graphs represent the mean ± SEM of the apical/basal fluorescence of the aliquots of collected from apical and basal chambers of the transwells. *$P < .05$, comparing the decrease in apical/basal flux in VEGF or CM treatment from 0 to 6 hours, one-way ANOVA. **$P < .01$, comparing the apical/basal flux between VEGF- or CM-treated and anti-uPAR antibody, Student's t test.

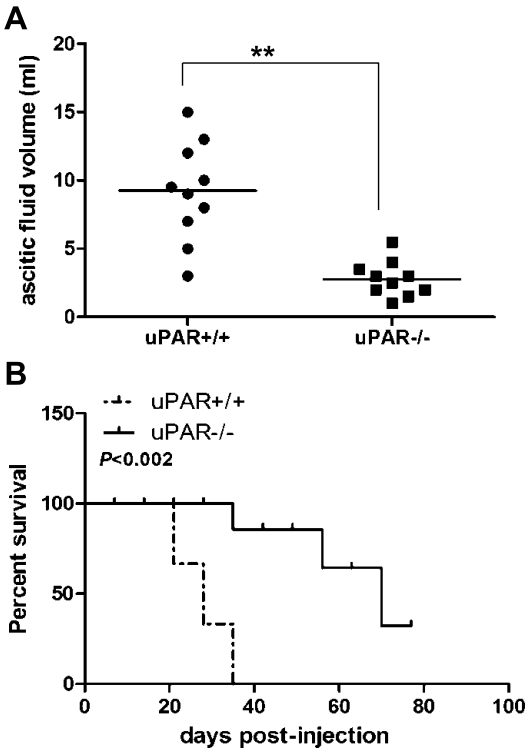

Figure W2. uPAR deficiency inhibits VEGF-induced intraperitoneal tumor growth and ascites fluid. (A) Scatterplots representing the incidence and volume of ascitic fluid measured in both genotypes at the end of 5 weeks after ID8 VEGF injection. Values represent mean ± SEM. *$P < .001$, comparing ascitic fluid volume between $uPAR^{-/-}$ and $uPAR^{+/+}$ mice. (B) Kaplan-Meier curve showing animal survival of $uPAR^{+/+}$ and $uPAR^{-/-}$ mice after IP injection of ID8-VEGF cells (1×10^6 cells/500 μl PBS).